Atomic Oxygen Erosion Resistance of Titania–Polyimide Hybrid Films Derived from Titanium Tetrabutoxide and Polyamic Acid

Fei Xiao, Kai Wang, Maosheng Zhan

Key Laboratory of Aerospace Materials and Performance (Ministry of Education), School of Materials Science and Engineering, Beihang University, No. 37, Xueyuan Road, Beijing 100191, PR China

Received 3 January 2011; accepted 2 March 2011
DOI 10.1002/app.34467
Published online 26 July 2011 in Wiley Online Library (wileyonlinelibrary.com).

ABSTRACT: A series of polyimide/titania (PI/TiO_2) hybrid films have been successfully synthesized based on titanium tetrabutoxide ($Ti(OEt)_4$), 3,3′,4,4′-bezonphenone tetracarboxylic dianhydride (BTDA), 4,4′-oxydianiline (ODA), and 1,3-bis(aminopropyl) tetramethyldisiloxane (APrTMOS) by a sol–gel process. The atomic oxygen (AO) exposure tests were carried out using a ground-based AO effects simulation facility. The chemical structure of PI/TiO_2 films was characterized by Fourier transform-infrared (FT-IR) spectroscope before and after AO exposure. The glass transition temperature (T_g) and mechanical properties were examined by dynamic mechanical analysis (DMA) and universal mechanical testing machine, respectively. The tensile strength and elongation of the hybrid film decreased with the increase of TiO_2 content, whereas the T_g increased with the increase of TiO_2 content. The effects of TiO_2 content on the morphology and structure evolvement of PI/TiO_2 hybrid films were also investigated using field emission scanning electron microscopy (FE-SEM) and X-ray photoelectron spectroscope (XPS), respectively. The results indicated that a TiO_2-rich layer resulting from the $Ti(OEt)_4$ formed on the PI film after AO exposure, which decreased the mass loss rate and obviously improved the AO resistance of PI films. © 2011 Wiley Periodicals, Inc. J Appl Polym Sci 123: 143–151, 2012

Key words: polyimide; titania; atomic oxygen; XPS; low earth orbit

INTRODUCTION

Various kinds of spacecraft traveling in low earth orbit (LEO), altitudes ranging from 100 km to 1000 km, where atomic oxygen (AO), ultraviolet (UV) radiation, vacuum ultraviolet (VUV) radiation, thermal cycling, and impact of small fragments are present, and these can break organic bonds. Many ground simulation experiments and in-orbit testing indicate that the principal component (AO) of the LEO environment have a strong impact on the performance of polymers.[1–6]

Aromatic polyimides (PIs) have a wide range of applications as high-performance materials in the aerospace industries because of their excellent properties such as tensile strength, modulus, thermal stability, and dielectric. However, the interaction of AO with PIs located at the outer surfaces of a spacecraft cause organic bond cleavage. The resulting bond cleavage can give rise to chain scission and/or crosslinking that cause physical, mechanical, and optical property changes in the polymers.[7–10]

Correspondence to: K. Wang (wangkai@buaa.edu.cn).

Journal of Applied Polymer Science, Vol. 123, 143–151 (2012)

Because of no commercially available PIs being resistant to degradation by AO irradiation, one approach is PIs protected from AO erosion by using a coating[11,12] or ion injection[13–15] to form a protective layer on the material surface. However, it is very difficult to fabricate a defect-free uniform AO protective coating. And the oxidation damage of the underlying polymer may proceed through pinhole and scratch defects by undercutting erosion.[16,17] The AO resistant polymer development has recently focused on copolymerization, blending, or hybrid technology to introduce AO resistant component such as silica-containing[18–22] or phosphorus-containing[23,24] component into the PI matrix. Therefore, a new protective layer can be formed even if there are some defects from manufacturing, transportation, or impact of small fragments.

During the past decades, organic–inorganic hybrid nanocomposites have received extensive interests from both the academic and industrial domain. Organic–inorganic hybrid PI films such as PI/SiO_2,[25–28] PI/Al_2O_3,[29] PI/titania (TiO_2),[30–32] and PI/V_2O_5[33] have been widely reported. And some of them have been evaluated as AO resistant coating or films.

In our previous work,[34] we developed a Zr-containing PI hybrid film which offer better AO

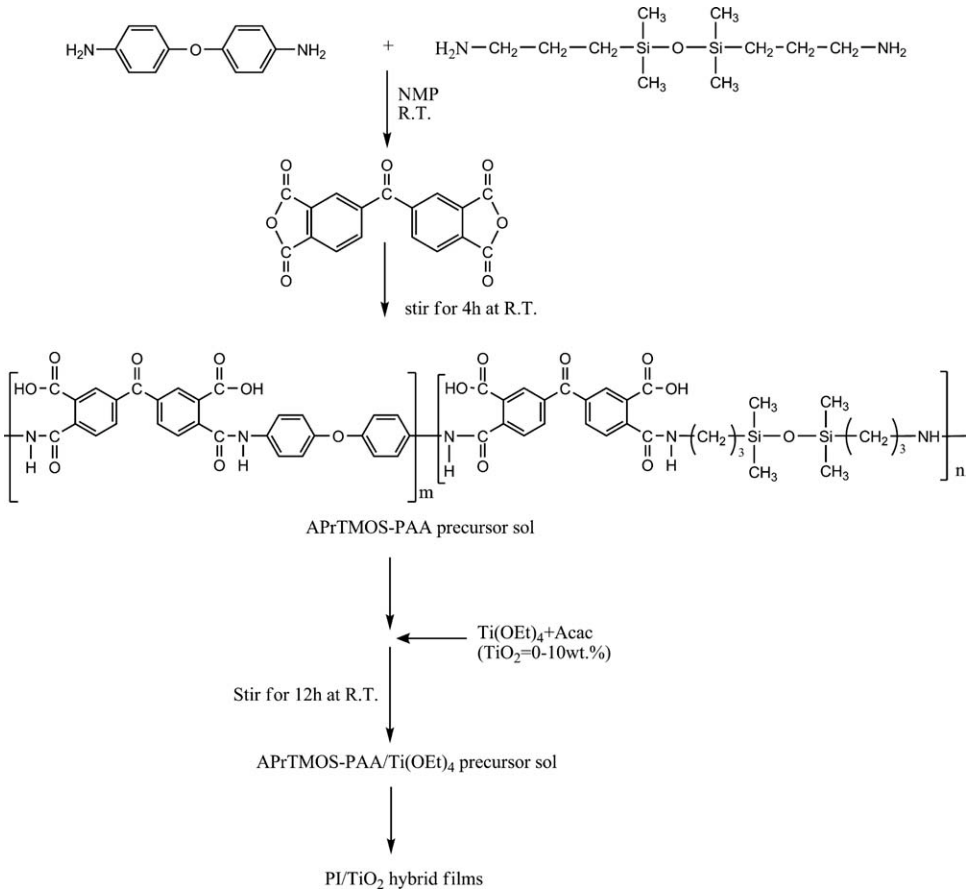

Figure 1 Flow chart of the procedures to prepare the PI/TiO_2 hybrid films.

resistance. We therefore hope that PI/TiO_2 hybrids could provide another way to make PI with desirable AO resistant properties. In this current work, a series of PI/TiO_2 hybrid films were synthesized by using a sol–gel process to study the effect of the composition on the morphology, thermal, mechanical, and AO resistant properties of the material. Titanium tetrabutoxide ($Ti(OEt)_4$) was chosen as a precursor for TiO_2. To maximize the interfacial compatibility between the organic and the inorganic phase, 1,3-bis(aminopropyl) tetramethyldisiloxane (APrTMOS) was introduced into the hybrid system. The AO erosion resistance was evaluated through AO exposure testing on our ground-based AO effects simulation facility. The effects of TiO_2 content on the morphology and structure evolvement of PI/TiO_2 hybrid films were investigated using field emission scanning electron microscopy (FE-SEM) and X-ray photoelectron spectrometer (XPS), respectively.

EXPERIMENTAL

Materials

$Ti(OEt)_4$ (Shanghai Shenzhong Fine Chemical Engineering Ltd., China), 4,4′-oxydianiline (ODA, Shanghai Chemical Reagent Corp., China), and APrTMOS (Alfa Aesar®, China) were used as received. 3,3′,4,4′-Bezonphenone tetracarboxylic dianhydride (BTDA, Beijing Multi. Tech. Co., Ltd., China) was dried in a vacuum oven at 150°C for 12 h prior to use. Acetylacetone (Acac, Guangdong Xilong Chemical Co., Ltd., China) was used as chelating agent to stabilize the titanium alkoxide. *N*-Methyl-2-pyrrolidone (NMP, Beijing Chemical Reagents Corp., China) as solvent was vacuum distilled and stored with 4 Å molecular sieves before use.

Preparation of PI/TiO_2 hybrid films

In this study, we prepared a series of PI/TiO_2 hybrid films by a sol–gel process as shown in Figure 1. ODA and NMP were added into a 250 mL three-neck round-bottom flask equipped with a magnetic stirrer, a nitrogen inlet, and a gas outlet. As to poly(amic acid) (PAA) with 10 wt % calculated TiO_2, after the ODA had dissolved completely, 0.19 g of APrTMOS was added into the flask dropwise under a nitrogen atmosphere. The mole ratio between ODA and APrTMOS was 0.98 : 0.02. The PAA solutions with a solid content of 20 wt % were obtained

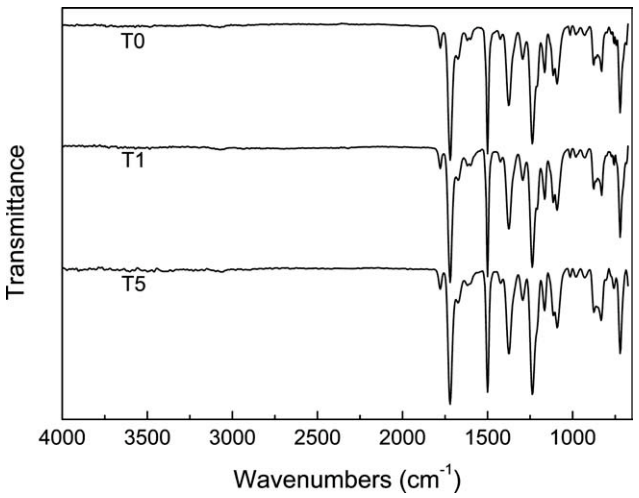

Figure 2 FT-IR spectra of PI/TiO_2 hybrid film T0, T1, and T5 before AO exposure.

by adding an equal mole of BTDA into the flask and stirring for at least 4 h at ambient temperature. Then 18.50 g of titanium precursor solution which was obtained from 1 mol of $Ti(OEt)_4$ and 4 mol of Acac was added into the flask dropwise under mechanical and ultrasonic agitation over a period of 60 min.

The freestanding films were made by casting the PAA solutions onto a dust free glass plate by an automatic film applicator. The resulting PAA thin films were then stepwise heated under an air atmosphere at 80, 120, 150, 200, 250, and 300°C, for 1h at each temperature. On cooling, the films were stripped off the glass surface by immersion of the glass plate into water. The hybrid films have an average thickness of 35–40 μm in final. The calculated TiO_2 concentration were approximately 0, 1, 3, 5, and 10 wt %, assuming complete imidization, complete conversion of the $Ti(OEt)_4$ to the TiO_2, and no residual solvent. The identification numbers of these hybrid films were T0, T1, T3, T5, and T10, respectively. The films are too brittle to strip off from the glass in one piece with the TiO_2 concentration about 10 wt % theoretical amount. The TiO_2 portions in the hybrid films were calculated by assuming that the sol–gel reaction proceeded completely.

Characterization

The Fourier transform infrared (FT-IR) spectra were recorded between 4000 and 400 cm^{-1} on a Nicolet NEXUS-470 spectrometer for PI and PI/TiO_2 hybrid film T0, T1, T3, and T5 before and after AO exposure. The mechanical properties of the solution-cast films were measured according to ISO 527-3-1995. The test specimens were prepared by cutting the films into 10-mm-wide strips with a total length of 120 mm with a drawing rate of 5 mm/min at room temperature. Dynamic mechanical analysis (DMA) was performed using a DMA-7e from Perkin–Elmer at heating rate of 5°C/min from RT to 300°C. A rectangular specimen of 50 × 5 × 0.04 mm^3 was used in the tensile geometry mode, at a frequency of 1 Hz. The glass transition temperature (T_g) was taken as the temperature at which tanδ showed a maximum. A minimum of five specimens were tested.

AO exposure experiment was performed by using a ground-based AO effects simulation facility with filament discharge oxygen plasma. The films were machined to the size of 1 cm ×1 cm squares before test. The samples were dried in vacuum oven at 200°C for 2 h to remove solvents. A 15 h AO exposure was carried out during which the samples were weighted at regular intervals to investigate the relationship of mass loss (ΔM) as a function of exposure time (t). As for the vacuum chamber, the working air pressure was 0.15 Pa, the discharging voltage was 120 V, and the discharging current of the lamp was 140 mA. AO accumulation flux was calculated by mass loss of standard commercial Kapton® H film with the following formula:

$$F = \Delta M/(\rho \cdot A \cdot \gamma) \quad (1)$$

where F indicates AO accumulation flux (atom/cm^2), ΔM is mass loss of film (g), ρ indicates material density (g/cm^3), A is sample area (cm^2), and γ is erosion rate of material (cm^3/atom). As for Kapton® H film, $\rho = 1.4$ g/cm^3 and $\gamma = 3 \times 10^{-24}$ cm^3/atom. AO accumulation flux in period of 15 h is 4.88×10^{20} atom/cm^2 which is equivalent to the AO accumulation flux of ~ 104 days at altitudes of 400 km.

The mass of the sample was measured with a DT-100 balance, sensitivity is $\pm 1.5 \times 10^{-5}$ g. A FE-SEM (American FEI corp., X.30S-FEG) was used to observe the surface morphology and aggregate structure of sample before and after AO irradiation. The fracture morphology was also examined using the FE-SEM.

An XPS (Japan ULVAC-PHI corp., PHI Quantera) with a Al Ka X-ray source was used to analyze the elemental composition and valence of the film surface before and after AO exposure. To compensate for surface charging effects, all binding energies (BEs) were referenced to the C 1s hydrocarbon peak at 284.8 eV.

RESULTS AND DISCUSSION

Infrared analysis

In the IR spectrum of Figure 2, the disappearance of amic acid absorptions at 1650–1700 cm^{-1}(C=ONH) and 2400–3400 cm^{-1} (C=OOH) in all spectra, together with the appearance of characteristic imide

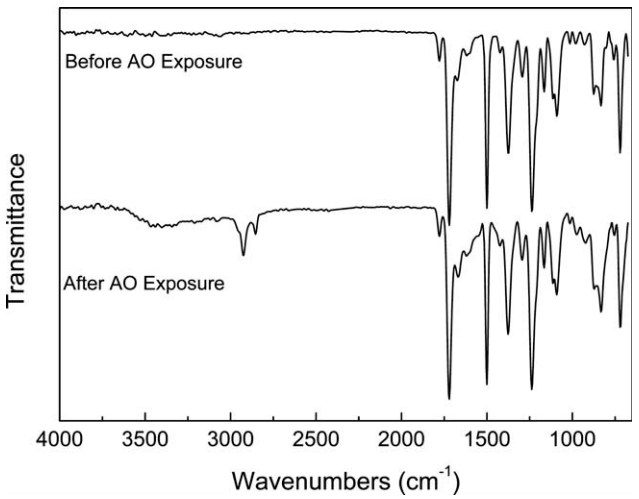

Figure 3 FT-IR spectra of PI/TiO_2 hybrid film T3 before and after AO exposure.

absorption bands at 1778 cm^{-1} (C=O asymmetric stretch) and 1720 cm^{-1} (C=O symmetric stretch), 1381 cm^{-1} (C—N stretch), 1110, and 720 cm^{-1} (imide ring deformation) indicate the transformation of *o*-carboxyl amide to the imide ring, therefore confirming the complete imidization of the PAA. Further, the disappeared of Ti—OH cm^{-1} (around 3400 cm^{-1}) indicate that most of the $Ti(OEt)_4$ has been converted into the Ti—O—Ti network. Accordingly, a broad absorption band in the vicinity of 400–850 cm^{-1} corresponds to the Ti—O—Ti network, and the intensity of this broad absorption band increased with increasing TiO_2 contents, which provided the evidence of the formation of the three-dimensional Ti—O—Ti network in the hybrid films.

Figure 3 illustrates the FT-IR spectra of the prepared PI–TiO_2 hybrid thin film T3 before and after AO exposure. From the curves of T3 before AO exposure, it can be seen that there are no absorption bands at 3000–3500 cm^{-1} which indicate that all Ti—OH has been converted to the inorganic phase composed of Ti—O—Ti linkages.

It is worth mentioning that with range of 3500–2500 cm^{-1}, absorption bands were found after AO exposure. Among that peaks, the new band at 3500–3000 is attributed to a small amount of Ti—OH and Si—OH. Also, the double peaks at 2950 and 2850 cm^{-1} represent —CH_2 asymmetrical stretch vibration and symmetrical stretch vibration. It is interesting that the relative absorption intensity of the Ti—O—Ti in the range of 400–850 cm^{-1} versus the cyclobenzene C (γ_{c-c}) has increased.

The SEM photos of T3 show the Ti—O—Ti 3D network on the outside surface of the hybrid film T3, and the block chain of —N—$(CH_2)_3$—$Si(CH_3)_2$—O—$Si(CH_3)_2$—$(CH_2)_3$—N— (APrTMOS) bonding the PI main chain was ruptured. Consequently, the —CH_2 peaks were obviously higher than that of PI/ZrO_2 hybrid film after AO experiment in our

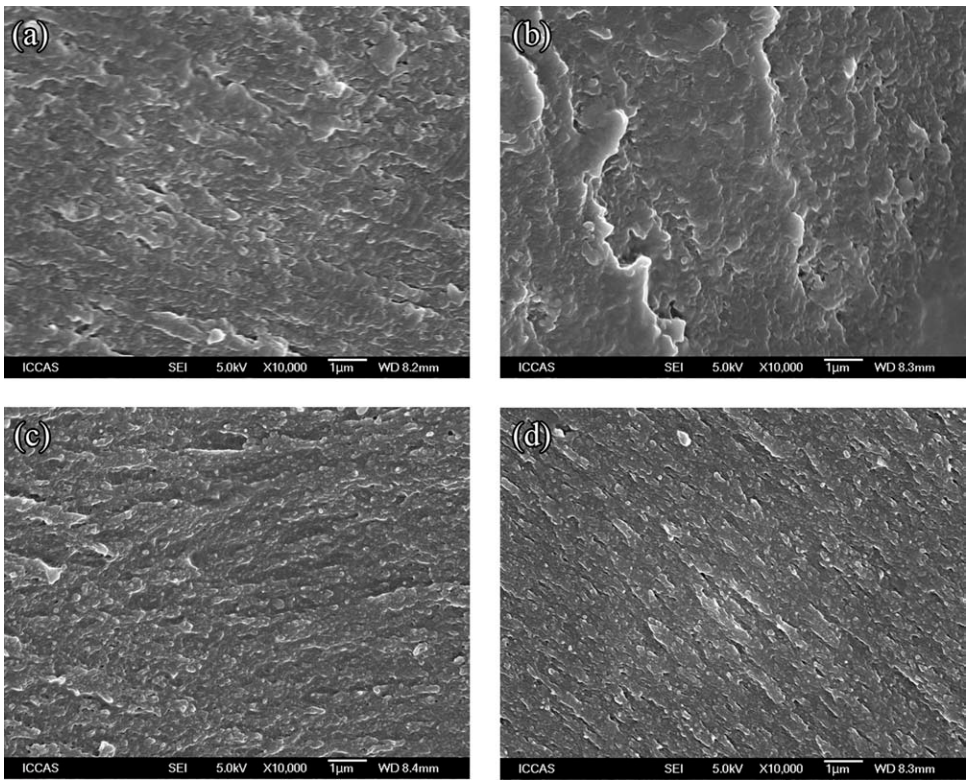

Figure 4 Fracture surface SEM images of PI and PI/TiO_2 hybrid films: scale bar: 1μm.

TABLE I
Mechanical and Thermal Properties of PI/TiO_2 Hybrid Films

Sample	Theoretical TiO_2 content (wt %)	T_g (°C)[a]	Tensile strength (MPa)	Modulus (GPa)	Elongation (%)
T0	0	298.1	127.0	3.4	6.5
T1	1	308.7	147.8	4.1	6.0
T3	3	324.2	81.9	3.7	2.4
T5	5	344.8	40.5	3.7	1.1
T10	10	—[b]	—	—	—

[a] Glass transition temperature determined by DMA.
[b] The film was too brittle to measure.

previous research.[34] During the AO attack, the PI main chain was attacked by AO to give rise to OH/H_2O. Hereafter, Si—OH and Ti—OH continued to form on the sample during the AO experiment.

Fracture surface morphology

The SEM micrographs of the fractured surface of hybrid film are shown in Figure 4. The distributions of TiO_2 and microphase separation were investigated. When the TiO_2 content is less than 1 wt %, the fractured surface is very smooth, and the inorganic particles of TiO_2 are scarcely seen from Figure 4(a,b). The hybrid films showed good compatibility between polymer matrix and the TiO_2 phase. However, when the TiO_2 content exceeded 3 wt %, the compatibility became worse. The micrograph of Figure 4(c,d) reveals that little particles of TiO_2 exist, indicating a very poor interfacial bond between the two phases.

Mechanical and thermal properties

The mechanical properties of the PI/TiO_2 hybrid thin film are presented in Table I. It is remarkable to observe that the tensile strength increases with increasing of the theoretical TiO_2 content up to 1 wt % and then reduces to 40.5 MPa with the increase of the theoretical TiO_2 content up to 5 wt %. The tensile strength increases by 16.4%, whereas the elongation at break decreases with the increase of TiO_2 content. The dependence of the moduli of all studied hybrid films on the TiO_2 content is shown in Table I. The moduli of the hybrid film represent a maximum with the TiO_2 content up to 1 wt %, and then beginning to reduce to 3.7 GPa and remaining the same up to 5 wt %. The film T10 was too brittle to test. The improvement of mechanical properties should be the results of the formation of the bonding site between the organic polymer phase and the inorganic phase, within a proper range of the crosslink density, the strain and toughness can be controlled.

The glass transition temperatures measured by dynamic mechanical-temperature relaxation behavior are shown in Table I. The presence of TiO_2 increases the T_g. The increase of the T_g may be attributed to the interfacial interaction and possible crosslinking between the PI and TiO_2. The results indicate that the mobility of the PI chains was restricted by the TiO_2 crosslinking sites. On the other hand, the increase in T_g values could indicate that the free volume of PI/TiO_2 hybrid film is much larger than that of the pure PI because of TiO_2 particles crosslinking sites.

Mass loss

A series of PI/TiO_2 hybrid films were prepared by a two-step approach based on BTDA, ODA, ArPTMOS, and $Ti(OEt)_4$. To study the effect of the introduction of TiO_2 on the AO resistant properties hybrid films, the ground-based AO exposure experiments were carried out. The mass loss of PI/TiO_2 hybrid films as a function of AO exposure time is shown in Figure 5. As exposure time goes on, not unexpectedly, the mass loss of Kapton® H increases

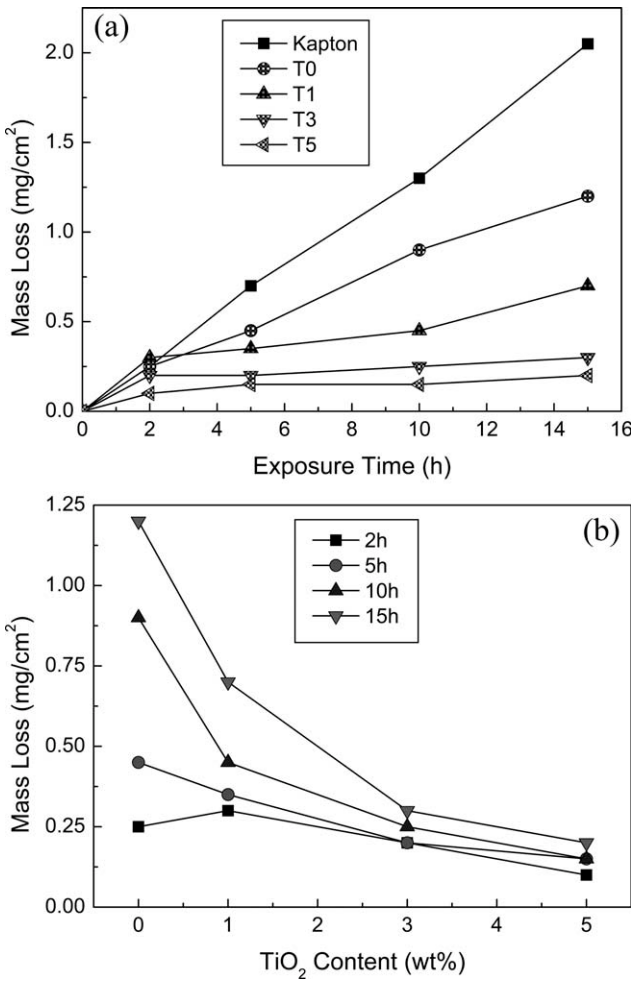

Figure 5 Mass loss of PI and PI/TiO_2 films as a function of (a) exposure time and (b) TiO_2 content during AO exposure.

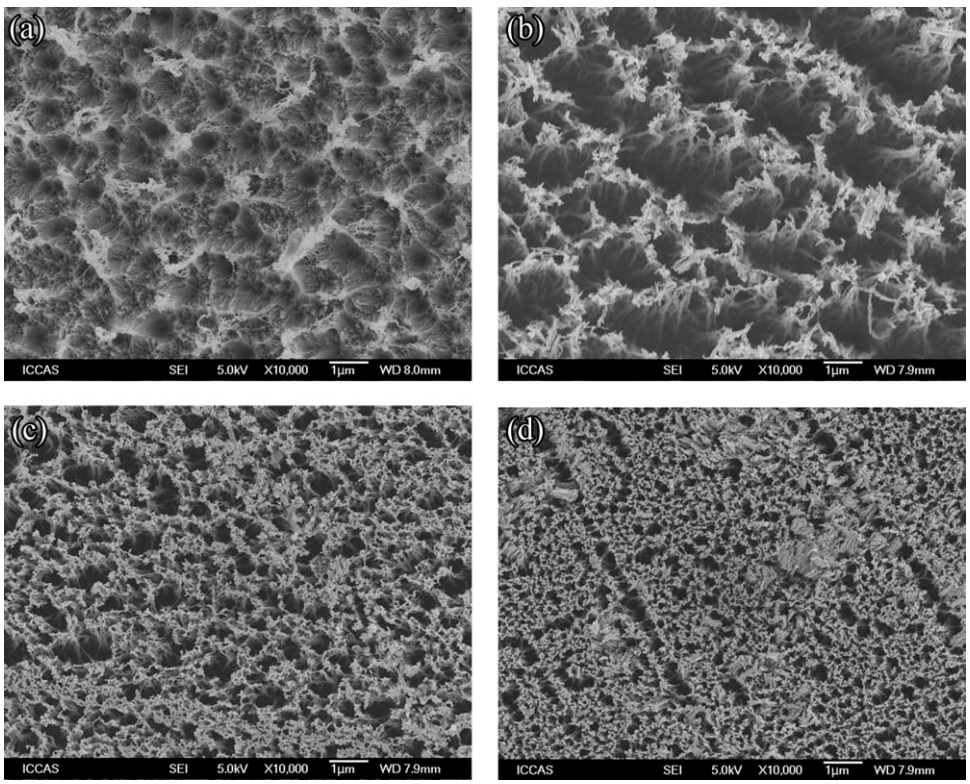

Figure 6 SEM surface morphologies of (a) T0, (b) T1, (c) T3, and (d) T5 after 15h AO exposure.

nearly with a linear erosion rate which indicate the Kapton has been eroded severely. However, it can be clearly seen from Figure 5(a) that the mass loss rate of PI/TiO_2 hybrid films decreases with increasing of the TiO_2 content. The mass loss decreases in the order of Kapton > T0 > T1 > T3 > T5. The mass loss of T3 and T5 exceeded 3 wt % theoretical TiO_2 content increases slowly with the increase of exposure time. When the TiO_2 content increased to 5 wt % (T5), the mass loss after 15 h AO exposure is decreased to 0.2 mg/cm^2, which is approximate 6% that of Kapton® H. It can be observed remarkably that 5h, 10h, and 15h curves demonstrate a decline tendency excluding 2h curve as shown in Figure 5(b). The mass loss of 2h curve slightly increases with increasing of TiO_2 content until 1 wt %. It could be that little TiO_2 might accelerate the degradation of film surface as catalyst via irradiation by lamp light in the vacuum chamber. These results indicate that one kind of enriched Ti protection layers form on the surface of the hybrid film prevent the further erosion. The higher TiO_2 contents exhibit better AO resistance.

Changes in surface morphology

Figure 6 illustrates the surface morphologies of T0, T1, T3, and T5 films after 15 h (4.88×10^{20} atom/cm^2) AO exposure. As shown in Figure 6(a), the surface of the films changes dramatically after 15h AO irradiation and exhibit a "hill-like" morphology with lots of micropores surrounding the "hill," indicates that they suffered serious erosion. This kind of morphology may be due to the "undercutting" effects of AO erosion, other studies have also shown obvious changes after AO exposure.[35–37] The reason for the changed surface morphology can be attributed to low molecular weight debris of polymers, CO, and CO_2 evacuated from the surface leaving holes below.

The surface morphology of PI/TiO_2 hybrid film T1 after 15 h AO exposure is shown in Figure 6(b), which is completely different from film T0. The surface of hybrid film T1 exhibits more holes and ravines, which can be ascribed to evacuate of CO_x and form of TiO_2 network initially. As for Figure 6(c,d), low "relief-like" morphology can be seen, which might be composed of the compact three-dimensional TiO_2 network. When the density of TiO_2 network reach to a certain amount, the morphology look more like a TiO_2-rich layer.

XPS analysis

The elemental composition of PI/TiO_2 hybrid film before and after AO exposure was calculated from the wide scan spectra as shown in Table II. The AO reaction taken place on the surface of the hybrid film T3 causes that the relative concentration of C

TABLE II
The Surface Composition of the PI/TiO_2 Hybrid Films T0 and T3 Before and After the AO Effects Experiment

Sample	T0		T3	
	Element concentration (%)			
Element peaks	Before AO exposure	After AO exposure	Before AO exposure	After AO exposure
C1s	75.10	75.14	78.65	59.04
O1s	19.87	21.93	18.10	31.93
N1s	5.03	2.93	3.26	0.57
Ti2p3	0.0	0.0	0.0	8.46

decreased from 78.65% to 59.04% and N from 3.26% to 0.57%, whereas the relative concentration of O increased from 18.10% to 31.93%. The concentration of Ti increased to 8.46% sharply. The incorporation of oxygen exceeds the loss of oxygen by evacuation of volatiles. The Ti oxides are nonvolatile and remain on the surface of the hybrid film, which results in an increase of Ti.

According to XPS standard spectra databases, theoretical composition and relative references,[38–42] the XPS spectra of the hybrid film was deconvoluted. The curve-fitting procedure including the addition of possible components, the area and positions of all components was carried out and then adjusted to obtain the best fit. The curve-fitting results of C 1s, O 1s, N 1s, and Ti 2p before and after AO irradiation are shown in Figure 7 and Table III.

First, Figure 7(a) shows the C 1s XPS spectra of T3 hybrid film before and after AO exposure. It is seen that the C 1s BE has no evidently shifts before and after AO exposure. The C 1s line consists of five components, the most intense peak at 284.8 eV, and the others weaker peaks at 284.3 eV, 285.4 eV, 286.1 eV, and 288.4 eV, respectively, before AO exposure. The first two peaks are usually assigned to C—H of the ODA molecular chain and imide phenyl ring, the peak at 285.4 eV is C*—C=O connected to the carbonyl carbon on the backbone of the polymer chain. The well-defined broad peak at 288.4 eV is due to carbonyl groups on the PI chain. The obvious changes are the intensity of all peaks almost decreases after AO exposure. To our surprise, the appearance of peak at 283.9 eV assigned to

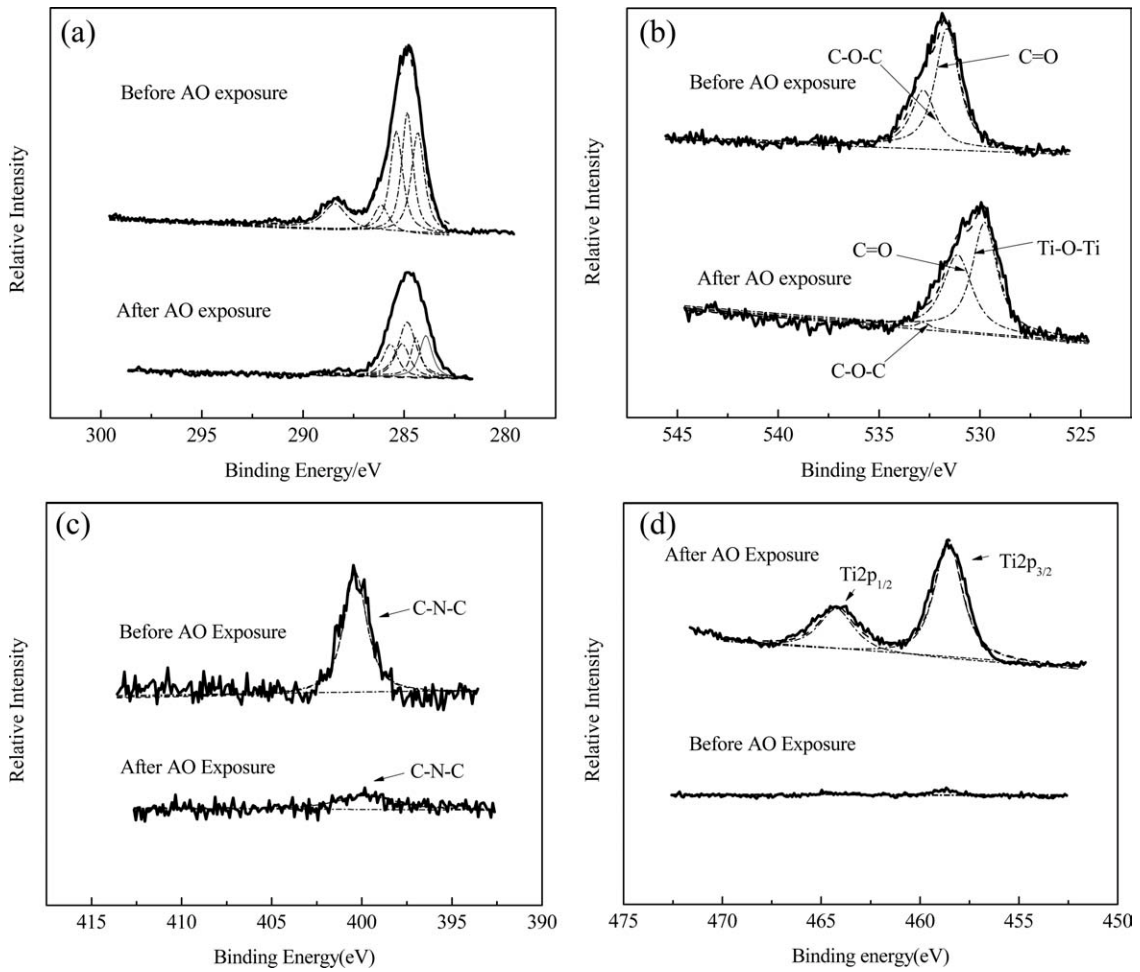

Figure 7 XPS spectra (a) C 1s, (b) O 1s, (c) N 1s, and (d) Ti 2p of T3 hybrid film before and after AO exposure.

TABLE III
XPS Surface Component Analysis of T3 Before and After AO Exposure

	Before AO exposure			After AO exposure		
Element peaks	Binding energy (eV)	Assignments	Area (%)	Binding energy (eV)	Assignments	Area (%)
C1s	—	—	—	283.9	Unsaturated	18.2
	284.3	C—H (imide phenyl ring)	26.7	284.4	C—H (imide phenyl ring)	12.4
	284.8	C—H (ODA phenyl ring)	27.7	284.8	C—H (ODA phenyl ring)	33.6
	285.4	C*—C=O	25.9	285.1	C*—C=O	17.5
	286.1	C—N, C—O	8.4	285.7	C—N, C—O	16.6
	288.4	C=O	11.3	288.3	C=O	1.6
O1s	—	—	—	529.8	TiO_2	54.2
	531.6	C=O	67.8	531.1	C=O	44.4
	532.8	C—O—C	32.2	532.8	C—O—C	1.4
N1s	400.3	C—N—C	100	399.7	C—N—C	100
Ti2p	—	—	—	458.6	$Ti2p_{3/2}$	69.1
				464.2	$Ti2p_{1/2}$	30.9

unsaturated C* may be ascribed to the saturated C on the phenyl ring changing into unsaturated C* via abstracting hydrogen reaction. These results indicate that C oxide volatiles are formed because of AO attacking weak sites of PI molecule chain.

Second, the deconvolution spectra of O 1s before and after AO exposure are shown in Figure 7(b). Unexpectedly, the peak corresponding to TiO_2 is not observed before AO exposure. The reasonable explanation is that the content of TiO_2 is too low. The BE at 531.6 eV is attributed to the oxygen of the C=O bond and at 532.8 eV is attributed to the C—O—C bond before AO exposure. As expected, the new peak at 530 eV is attributed to the TiO_2 appearance after AO exposure, whereas the relative O element concentration increases. It can be concluded that the TiO_2 layer forms on the surface of the film. The BE of N elements before and after AO exposure is shown in Figure 7(c). Both peaks show the similar shape around 400 eV, which is assigned to the N on the PI. The BE of N has no obvious shifts, whereas the intensity of the peak decreases after AO exposure. A weak peak is observed in this current work for the C—N—C peak located at 400.2 eV, it disappeared in all spectra of PI/ZrO_2 hybrid film in our previous study. It could be partial cleavage of the imide ring.

The curve-fitting N 1s indicates a decrease in concentrations of nitrogen in the imide ring. Incorporation of C 1s and O 1s suggests that the imide rings are indeed the weakest bonds which undergo substantial changes during AO exposure.

In addition to the above changes, the BE of Ti element before and after AO exposure is compared, as shown in Figure 7(d). Prior to AO exposure, the lack of Ti 2p peaks in this spectra is suggestive of the content of TiO_2 less than detecting inferior limitation of XPS (0.1% atom concentration). Besides, the probe depth of XPS (approximate 7–10 nm) should be taken into account. AO exposure causes appearance of two new peaks location at 458.6 eV and 464.2 eV of the main component of Ti 2p. Incorporation with the Ti—O—Ti peak in the O1s line indicates the existence of a considerable amount of TiO_2 on the surface of the PI/TiO_2 film.

CONCLUSIONS

In this paper, the PI/TiO_2 hybrid films have been successfully synthesized using sol–gel process with TiO_2 concentration up to 10 wt %, followed by thermal imidization. The chelating agent, Acac, was used to reduce the gelation rate of titanium alkoxide. Such a composite design afforded the films outstanding degradation resistance behavior in a space-simulating AO environment. The AO resistant properties of PI/TiO_2 hybrid films increased with the increase of TiO_2 contents. The mass loss of PI/TiO_2 hybrid films shows nonlinear character; when the content of TiO_2 reached 5 wt %, the mass loss of PI/TiO_2 hybrid film reduces to 6% of Kapton® H film. In AO exposure environment, it can be concluded that C—N bond will react with AO preferentially, which results in the scission of the molecular chain of PI and the formation of volatiles resulting in the mass loss. Although hydrogen cannot be observed in the XPS spectra, it most likely reacts rapidly with the AO to form water which desorbs. The TiO_2 is proved to play a key role preventing the erosion by AO by forming a TiO_2-rich protective layer on the film surface. The combination of higher glass transition temperature and improved AO resistance makes these films promising polymers for potential space applications in LEO.

The authors thank the National Nature Science Foundation of China for the financial support (No. 50803003). The authors also thank Prof. Xiao-Hu Zhao for the help in the oxygen plasma resistance test.

References

1. Banks, B. A.; de Groh, K. K.; Miller, S. K. R. NASA/TM-2004-213400, 2004.
2. Gittemeier, K. A.; Hawk, C. W. C. AIAA-2005-660, 2005.
3. Duo, S. W.; Li, M. S.; Zhang, Y. M. J Corrs Sci Technol Prot 2002, 14, 152.
4. Zhan, Y. Z.; Zhang, G. D. J Aerosp Mater Technol 2003, 1, 1.
5. Shen, L. J Chin Space Sci Technol 1994, 5, 54.
6. Watson, K. A.; Connell, J. W. R. NASA-2000-45sample-Kaw, 2000.
7. Dooling, D.; Finckenor, M. M. R. NASA/TP-1999-209260, 1999.
8. Kamenelzky, R. R.; Vaughn, J. A.; Finckenor, M. M.; Linton, R. C. R. NASA-TP-3595, 1995.
9. Hammoud, A. N.; Stavnes, M. W. R. NASA-198372, 1983.
10. Gulino, D. A. R. NASA-CR-195904, 1959.
11. Liu, X. P.; Tong, J. Y.; Li, J. H. J Spacecr Environ Eng 2006, 23, 39.
12. Devapal, D.; Packirisamy, S.; Korulla, R. M. J Appl Polym Sci 2004, 94, 2368.
13. Duo, S. W.; Li, M. S.; Zhou, Y. C.; J Trans Nonferr Metal Soc 2006, 16, 661.
14. Iskanderova, Z. Kleiman, J. Gudimenko, Y. J Nucl Instrum Meth B 1997, 127–128, 702.
15. Wang, X.; Zhao, X. H. J Nucl Instrum Meth B 2006, 243, 320.
16. de Groh, K. K.; Banks, B. A.; Demko, R. R. NASA/TM-2002-211479, 2002.
17. Snyder, A.; de Groh, K. K. R. NASA/TM-2001-210596, 2001.
18. Duo, S. W.; Li, M. S. J Surf Coat Technol 2006, 200, 6671.
19. Ryo, T. J Chem Mater 2003, 15, 793.
20. Wright, M. E.; Petteys, B. J.; Guenthner, A. J. J Macromol 2006, 39, 4710.
21. Verker, R.; Grossman, E.; Eliaz, N. J Acta Mater 2009, 57, 1112.
22. Phillips, S. H.; Haddad, T. S.; Tomczak, S. J. J Curr Opin Solid State Mater Sci 2004, 8, 21.
23. Watson, K. A.; Palmieri, F. L.; Connell, J. W. J Macromol 2002, 35, 4968.
24. Lin, C. H.; Lin, C. H. J Polym Sci Pol Chem 2007, 45, 2897–2912.
25. Kamenetzky, R. R.; Linton, R. C.; Finckenor, M. M.; Vaughn, J. A. C. AIAA-93-4103, 1993.
26. Cheng, S.; Shen, D. Z.; Zhu, X. S.; Tian, X. G.; Zhou, D. Y.; Fan, L. J. J Eur Polym Mater 2009, 45, 2767.
27. Duo, S. W.; Li, M. S.; Zhu, M.; Zhou, Y. C. J Surf Coat Technol 2006, 200, 6671.
28. Wang, X.; Zhao, X. H.; Wang, M. Z.; Shen, Z. G. J Nucl Instrum Meth B 2006, 243, 320.
29. Zhang, Y. H.; Li, Y.; Fu, S. Y.; Xin, J. H.; Daoud, W. A.; Li, L. F. J Polymer 2005, 46, 8373.
30. Musto, P.; Ragosta, G.; Scarinzi, G.; Mascia, L. J Polymer 2004, 45, 1697.
31. Ma, P. C.; Nie, W.; Yang, Z. H.; Zhang, P. H.; Li, G.; Lei, Q. Q.; Gao, L. X.; Ji, X. L.; Ding, M. X. J Appl Polym Sci 2008, 108, 705.
32. Tsai, M. H.; Liu, S. J.; Chiang, P. C. J Thin Solid Films 2006, 515, 1126.
33. Chiang, P. C.; Whang, W. T.; Tsai, M. H.; Wu, S. C. J Thin Solid Films 2004, 447–448, 359.
34. Xiao, F.; Wang, K.; Zhan, M. S. J Appl Surf Sci 2010, 256, 7384.
35. Kong, Y.; Du, H. W.; Yang, J. R.; Shi, D. Q.; Wang, Y. F.; Zhang, Y. Y.; Xin, W. Desalination 2002, 146, 49.
36. Tsai, M. H.; Huang, S. L.; Chen, P. J.; Chiang, P. C.; Chen, D. S.; Lu, H. H.; Chiu, W. M.; Chen, J. C.; Lu, H. T. Desalination 2008, 233, 232.
37. Zhang, X.; Wu, Y.; Liu, G.; He, S.; Yang, D. Thin Solid Films 2008, 516, 5020.
38. Shimamura, H.; Nakamura, T. Polymer Degrad Stabil 2009, 94, 1389.
39. Wohl, C. J.; Belcher, M. A.; Ghose, S.; Connell, J. W. Appl Surf Sci 2009, 255, 8135.
40. Li, C. D.; Zhou, S. F.; Yang, Y. D. J Spacecr Environ Eng 2009, 26, 9.
41. Wang, L. H.; Tian, Y.; Ding, H. Y. J Eur Polym Mater 2006, 42, 2921.
42. Pei, X. Q.; Li, Y.; Wang, Q. H.; Sun, X. J. J Appl Surf Sci 2009, 255, 5932.